Electronic, Magnetic, Redox, and Ligand-Binding Properties of $[MFe_3S_4]$ Clusters (M = Zn, Co, Mn) in *Pyrococcus furiosus* Ferredoxin

Michael G. Finnegan,[†] Richard C. Conover,[†] Jae-Bum Park,[‡] Zhi Hao Zhou,[‡] Michael W. W. Adams,[‡] and Michael K. Johnson*[,†]

Departments of Chemistry and Biochemistry and Center for Metalloenzyme Studies, University of Georgia, Athens, Georgia 30602

Received May 19, 1995[⊗]

The ground and excited state properties and ligand-binding capabilities of $[ZnFe_3S_4]^{2+,+}$, $[CoFe_3S_4]^{2+,+}$, and $[MnFe_3S_4]^{+}$ clusters in *Pyrococcus furiosus* Fd have been investigated by the combination of EPR, variable-temperature magnetic circular dichroism (VTMCD), and MCD magnetization studies. The ground state spins, $S = {}^5/_2$ for $[ZnFe_3S_4]^{+}$, $S = 2$ for $[ZnFe_3S_4]^{2+}$, $S = 1$ for $[CoFe_3S_4]^{+}$, $S = {}^1/_2$ for $[CoFe_3S_4]^{2+}$, and $S = 0$ for $[MnFe_3S_4]^{+}$, are consistent with a simple coupling scheme involving antiparallel interaction between the high-spin divalent metal ion and an $S = {}^5/_2$ $[Fe_3S_4]^{+}$ or $S = 2$ $[Fe_3S_4]^{0}$ cluster fragment. Redox potentials (*vs* NHE) were determined by dye-mediated EPR titrations at pH 7.6, $E_m = -241 \pm 20$ mV for $[ZnFe_3S_4]^{2+,+}$, $E_m = -163 \pm 10$ mV for $[CoFe_3S_4]^{2+,+}$, and $E_m > -100$ mV for $[MnFe_3S_4]^{2+,+}$, indicating that the potentials for $[MFe_3S_4]^{2+,+}$ clusters in *P. furiosus* Fd are ordered M = Fe < Zn < Co < Mn or Ni. On the basis of changes in EPR and/or VTMCD spectra, evidence is presented for cyanide binding at the unique metal site of the $[ZnFe_3S_4]^{+}$ and $[CoFe_3S_4]^{+}$ clusters and for 2-mercaptoethanol binding at the Zn site of the $[ZnFe_3S_4]^{+}$ cluster. The ground and excited state properties of the thiolate-bound $[ZnFe_3S_4]^{+}$ cluster in *P. furiosus* Fd are very similar to those of the equivalent cluster in *Desulfovibrio gigas* FdII, indicating coordination of the Zn by the indigenous cysteinate in this protein. The site specific reactivity, intracluster magnetic interactions, and redox properties of heteronuclear cubanes in general are discussed in light of these results.

Introduction

Homometallic cubane-type $[Fe_4S_4]$ clusters are one of the most pervasive electron transfer centers in biology and are found in ferredoxins (Fds)[1] as well as numerous soluble and membrane-bound metalloenzymes.[2] In addition, they constitute the active sites of several (de)hydratases[3] and their important role in determining protein structure[4] has made them candidates for biological sensors for oxygen[5] and iron.[6] Heterometallic cubane-type clusters of the type $[MFe_3S_4]$ where M is a metal other than Fe have been extensively investigated over the past decade in order to explore site-specific reactivity and to understand intracluster magnetic interactions. Moreover, although discrete heteronuclear clusters of this type have yet to be found in biology, the nitrogenase active site cluster can be considered as cubane-type $[MoFe_3S_3]$ and $[Fe_4S_3]$ fragments bridged by three μ_2-S^{2-} bridges.[7] Holm and co-workers have synthesized and characterized a range of crystallographically defined heterometallic clusters with $[MFe_3S_4]$ cores (M = Ni, Co, Mo, W, V, Re, Nb),[8] and the ability of some biological Fe_3S_4 clusters to take up exogenous metals has led to the formation of $[MFe_3S_4]$ clusters (M = Zn,[9−11] Co,[12,13] Ni,[13−15] Cd,[10,13,16] Ga,[15] Tl,[17,18] Cu[19]) in several low molecular weight bacterial ferredoxins (Fds).

Pyrococcus furiosus Fd is a small (M_r = 7500) hyperthermostable protein containing a single $[Fe_4S_4]$ cluster that

* Corresponding author. Telephone: 706-542-9378. FAX: 706-542-2353. E-mail: johnson@sunchem.chem.uga.edu.
[†] Department of Chemistry.
[‡] Department of Biochemistry.
[⊗] Abstract published in *Advance ACS Abstracts,* October 1, 1995.

(1) Abbreviations used: Fd(s), ferredoxin(s); (VT)MCD, (variable-temperature) magnetic circular dichroism; ENDOR, electron−nuclear double resonance; NHE, normal hydrogen electrode; 2-ME, 2-mercaptoethanol; Smes, 2,4,6-trimethylbenzenethiolate; Stib, 2,4,6-triisopropylbenzenethiolate.

(2) For recent reviews see: (a) Johnson, M. K. In *Encyclopedia of Inorganic Chemistry*; King, R. B., Ed.; Wiley: Chichester, 1994; Vol. 4; pp 1896−1915. (b) Cammack, R. *Adv. Inorg. Chem.* **1992**, *38*, 281−322.
(3) (a) Beinert, H.; Kennedy, M. C. *Eur. J. Biochem.* **1989**, *186*, 5−15. (b) Kennedy, M. C.; Stout, C. D. *Adv. Inorg. Chem.* **1992**, *38*, 323−340. (c) Flint, D. H.; Emptage, M. H.; Finnegan, M. G.; Fu, W.; Johnson, M. K. *J. Biol. Chem.* **1993**, *268*, 14732−14742 and references therein.
(4) Kuo, C.-F.; McRee, D. E.; Fisher, C. L.; O'Handley, S. F.; Cunningham, R. P.; Tainer, J. A. *Science* **1992**, *258*, 434−440.
(5) (a) Switzer, R. L. *BioFactors* **1989**, *2*, 77−86. (b) Smith, J. L.; Zaluzec, E. J.; Wery, J.-P.; Niu, L.; Switzer, R. L.; Zalkin, H.; Satow, Y. *Science* **1994**, *264*, 1427−1433.
(6) Haile, D. J.; Rouault, T. A.; Harford, J. B.; Kennedy, M. C.; Blodin, G. A.; Beinert, H.; Klausner, R. D. *Proc. Natl. Acad. Sci. U.S.A.* **1992**, *89*, 11735−11739.
(7) (a) Kim, J.; Rees, D. C. *Science* **1992**, *257*, 1677−1682. (b) Chan, M. K.; Kim, J.; Rees, D. C. *Science* **1993**, *260*, 792−794.
(8) Holm, R. H. *Adv. Inorg. Chem.* **1992**, *38*, 1−71.
(9) Surerus, K. K.; Münck, E.; Moura, I.; Moura, J. J. G.; LeGall, J. *J. Am. Chem. Soc.* **1987**, *109*, 3805−3807.
(10) Butt, J. N.; Armstrong, F. A.; Breton, J.; George, S. J.; Thomson, A. J.; Hatchikian, E. C. *J. Am. Chem. Soc.* **1991**, *113*, 6663−6670.
(11) Srivastava, K. K. P.; Surerus, K. K.; Conover, R. C.; Johnson, M. K.; Park, J.-B.; Adams, W.; Münck, E. *Inorg. Chem.* **1993**, *32*, 927−936.
(12) Moura, I.; Moura, J. J. G.; Münck, E.; Papaefthymiou, V.; LeGall, J. *J. Am. Chem. Soc.* **1986**, *108*, 349−351.
(13) Moreno, C.; Macedo, A. L.; Moura, I.; LeGall, J.; Moura, J. J. G. *J. Inorg. Biochem.* **1994**, *53*, 219−234.
(14) Conover, R. C.; Park, J.-B.; Adams, M. W. W.; Johnson, M. K. *J. Am. Chem. Soc.* **1990**, *112*, 4562−4564.
(15) Surerus, K. K. Ph.D. Thesis, University of Minnesota, Minneapolis, MN, 1989.
(16) Münck, E.; Papaefthymiou, V.; Surerus, K. K.; Girerd, J.-J. In *Metal Clusters in Proteins*; Que, L., Jr., Ed.; ACS Symposium Series 372; American Chemical Society: Washington, DC, 1988; pp 302−325.
(17) Butt, J. N.; Sucheta, A.; Armstrong, F. A.; Breton, J.; Thomson, A. J.; Hatchikian, E. C. *J. Am. Chem. Soc.* **1991**, *113*, 8948−8950.
(18) Fu, W.; Telser, J.; Hoffman, B. M.; Smith, E. T.; Adams, M. W. W.; Finnegan, M. G.; Conover, R. C.; Johnson, M. K. *J. Am. Chem. Soc.* **1994**, *116*, 5722−5729.
(19) Butt, J. N.; Niles, J.; Armstrong, F. A.; Breton, J.; Thomson, A. J. *Nature Struct. Biol.* **1994**, *1*, 427−433.

0020-1669/95/1334-5358$09.00/0

undergoes extremely facile $[Fe_4S_4] \leftrightarrow [Fe_3S_4]$ interconversion due, at least in part, to non-cysteinyl coordination at a specific Fe.[20,21] Recent ^{1}H-NMR[22] and ^{1}H-ENDOR[23] results indicate that the removable Fe is coordinated by the aspartate that replaces cysteine in the characteristic $C-X_2-C/D-X_2-C-X_n-CP$ arrangement of coordinating cysteines. Thus far, we have characterized the electronic and magnetic properties of $[MFe_3S_4]^{n+}$ clusters in *P. furiosus* Fd where M = Fe (n = 1, 2),[20] Zn (n = 1),[10] Ni (n = 1),[14] and Tl (n = 1, 2)[18] and compared them with similar clusters in *Desulfovibrio gigas* FdII,[9,12,13,15,16] *Thermococcus litoralis* Fd,[24] and *Desulfuricans africanus* FdIII.[10,17,19] On the basis of sequence considerations, the incorporated metal site is likely to have cysteinyl coordination in *D. gigas* FdII and *T. litoralis* Fd as opposed to aspartyl coordination in *P. furiosus* Fd and *D. africanus* FdIII. The difference in indigenous cluster ligation is also reflected in the ability of the clusters in *P. furiosus* Fd and *D. africanus* FdIII to bind exogenous ligands. Spectroscopic (EPR, ENDOR, and VTMCD) studies have provided unambiguous evidence for cyanide binding to $[Fe_4S_4]^+$ clusters in *P. furiosus* Fd,[23,25] and electrochemical studies indicate thiolate binding to $[Fe_4S_4]^{2+,+}$ clusters in *D. africanus* FdIII.[26] EPR and Mössbauer studies have also provided strong evidence for cyanide binding at the Ni site of the $[NiFe_3S_4]^+$ clusters in *P. furiosus* Fd.[11,14]

Here we report on the electronic, magnetic, redox, and ligand-binding properties of $[MFe_3S_4]^{2+,+}$ clusters (M = Zn, Co, Mn) in *P. furiosus* Fd as revealed by the combination of EPR and VTMCD studies. The results establish for the first time the magnetic ground state properties of $[MnFe_3S_4]^+$ and $[CoFe_3S_4]^+$ clusters, provide evidence for exogenous ligand binding to the $[ZnFe_3S_4]^+$ and $[CoFe_3S_4]^+$clusters in *P. furiosus* Fd, and facilitate comparison of the redox potentials for $[MFe_4S_4]^{2+,+}$ clusters (M = Fe, Zn, Co, Ni, Mn) in *P. furiosus* Fd. The site-specific reactivity, intracluster magnetic interactions, and redox properties of heteronuclear cubanes in general are discussed in light of these new results.

Materials and Methods

Sample Preparation. *P. furiosus* was grown and the ferredoxin was purified anaerobically in the presence of 2 mM sodium dithionite as previously described.[27] The form containing a $[Fe_3S_4]^+$ cluster was prepared by incubating the air-oxidized Fd with a 5-fold excess of potassium ferricyanide and a 10-fold excess of EDTA at room temperature for 30 min, followed by gel filtration (Sephadex G-25) to remove excess reagents. Sample concentrations for the Fd containing a $[Fe_3S_4]^+$ cluster were based on protein determinations[28] using apoprotein prepared by precipitation with trichloroacetic acid and/or EPR spin quantitations. These methods agreed to within ±10%. Preparation of the heterometallic clusters in *P. furiosus* Fd closely followed the procedures developed for *D. gigas* FdII,[9,12] and all procedures were carried out in a glovebox (Vacuum Atmospheres) under an Ar atmosphere with < 1 ppm O_2.

Samples of *P. furiosus* Fd containing $[ZnFe_3S_4]^+$, $[CoFe_3S_4]^+$, or $[MnFe_3S_4]^+$ clusters were obtained by anaerobic addition a 10-fold stoichiometric excess of $Zn(NO_3)\cdot xH_2O$ (99.999%, Aldrich Chemical Co.), $Co(NO_3)_2\cdot 6H_2O$ (99.999%, Aldrich Chemical Co.), or $Mn(OOCCH_3)_2\cdot 4H_2O$ (99.99%, Aldrich Chemical Co.) to the $[Fe_3S_4]^0$ form of the Fd in a 100 mM Mes buffer, pH 6.3, containing 2 mM sodium dithionite. The samples were incubated at room temperature for 30 min, followed by treatment with 10 mM EDTA, exchanging the buffer to 50 mM Tris/HCl, pH 7.8, with 2 mM dithionite, and removal of excess metal and EDTA by gel filtration (Sephadex G-25) or ultrafiltration using and Amicon unit fitted with a YM5 membrane. Metal analyses using inductively coupled plasma emission spectroscopy for three distinct samples of each heterometallic Fd gave 3.0 ± 0.3 Fe atoms/molecule and 1.4 ± 0.2 Zn atoms molecule for the $[ZnFe_3S_4]$ Fd, 3.0 ± 0.3 Fe atoms/molecule and 1.3 ± 0.2 Co atoms/molecule for the $[CoFe_3S_4]$ Fd, and 3.3 ± 0.4 Fe atoms/molecule and 1.3 ± 0.3 Mn atoms/molecule for the $[MnFe_3S_4]$ Fd. For the exogenous ligand-binding studies, anaerobic samples the Fd containing $[MFe_3S_4]^+$ clusters (M = Zn, Co, Mn) in 100 mM Tris/HCl, pH 7.8 (cyanide-binding studies), or 100 mM CAPS/NaOH, pH 11.0 (thiolate binding studies), were incubated for 5 min to 1 h with a 1- to-500-fold excess of neutralized potassium cyanide solution or 2-mercaptoethanol. Where necessary, the excess ligand was removed by anaerobic gel flitration (Sephadex G-25) under anaerobic conditions in the presence of 2 mM sodium dithionite. Samples of *D. gigas* FdII containing a $[ZnFe_3S_4]^+$ cluster were supplied by Drs. Eckard Münck and Kristene Surerus.

Attempts to oxidize the heterometallic clusters were carried out after removal of excess dithionite and in the presence of a 10-fold excess of Zn^{2+}, Co^{2+}, or Mn^{2+}, using a stoichiometric amount of ferricyanide or thionin under anaerobic conditions. EPR-monitored redox titrations were performed at ambient temperature (25−27 °C) in a glovebox under anaerobic conditions (<5 ppm of O_2) using a 50 mM Tris/HCl buffer, pH 7.5, and the method described by Dutton.[29] Mediator dyes were added, each to a concentration of ca. 50 μM, in order to cover the desired range of redox potentials, i.e. methyl viologen, benzyl viologen, neutral red, safranin, phenosafranin, phenoquinone, anthraquinone-2-sulfonate, anthraquinone-1,5-disulfonate, 2-hydroxy-1,4-naphthoquinone, 1,4-naphthoquinone, indigodisulfonate, methylene blue, 1,2-naphthoquinone, duroquinone, and 1,2-naphthoquinone-4-sulfonate. Methyl viologen, benzyl violgen, and phenosafranin were omitted for redox titrations of the Fd containing $[CoFe_3S_4]^{2+,+}$ clusters to avoid interference in the g = 2 region with radical species. Samples were first reduced completely by addition of excess sodium dithionite followed by oxidative titration with stock solutions of potassium ferricyanide or thionin in the same buffer. After equilibration at the desired potential, a 0.2-mL aliquot was transferred to a calibrated EPR tube and immediately frozen in liquid nitrogen. Potentials were measured with a platinum working electrode and a saturated calomel reference electrode and are reported relative to the normal hydrogen electrode (NHE).

Spectroscopic Measurements. Variable-temperature and variable-field MCD measurements were recorded on samples containing 50% (v/v) ethylene glycol using a Jasco J-500C spectropolarimeter mated to an Oxford Instruments SM3 split-coil superconducting magnet. The experimental protocols for measuring MCD spectra of oxygen-sensitive samples at fixed temperatures over the range 1.5−300 K with magnetic fields up to 5 T have been described elsewhere.[30] X-band EPR spectra were recorded on a Bruker ESP-300E EPR spectrometer equipped with a ER-4116 dual-mode cavity and an Oxford Instruments ESR-9 flow cryostat. Spin quantitations were carried out under nonsaturating conditions using 1 mM CuEDTA as the standard. Spectral simulations were performed using the Simfonia software package (Bruker Instrument Co.).

Results

$[MnFe_3S_4]^+$ Clusters in *P. furiosus* Fd. Addition of a 10-fold excess of Mn^{2+} had no effect on the absorption spectrum of the *P. furiosus* Fd containing a $[Fe_3S_4]^+$ cluster. However, analogous treatment of the reduced Fd containing a $[Fe_3S_4]^0$

(20) Conover, R. C.; Kowal, A. T.; Fu, W.; Park, J.-B.; Aono, S.; Adams, M. W. W.; Johnson, M. K. *J. Biol. Chem.* **1990**, *265*, 8533−8541.
(21) Busse, S. C.; La Mar, G. N.; Yu, L.-P.; Howard, J. B.; Smith, E. T.; Zhou, Z. H.; Adams, M. W. W. *Biochemistry* **1992**, *31*, 11952−11962.
(22) Calzolai, L.; Gorst, C. M.; Zhao, Z.-H.; Teng, Q.; Adams, M. W. W.; La Mar, G. N. *Biochemistry*, in press.
(23) Telser, J.; Smith, E. T.; Adams, M. W. W.; Conover, R. C.; Johnson, M. K.; Hoffman, B. M. *J. Am. Chem. Soc.* **1995**, *117*, 5133−5140.
(24) Hankins, H. L. M.S. Thesis, University of Georgia, Athens, GA, 1994.
(25) Conover, R. C.; Park, J.-B.; Adams, M. W. W.; Johnson, M. K. *J. Am. Chem. Soc.* **1991**, *113*, 2799−2800.
(26) Butt, J. N.; Sucheta, A.; Armstrong, F. A.; Breton, J.; Thomson, A. J.; Hatchikian, E. C. *J. Am. Chem. Soc.* **1993**, *115*, 1413−1421.
(27) Aono, S.; Bryant, F. O.; Adams, M. W. W. *J. Bacteriol.* **1989**, *171*, 3433−3439.
(28) Lowery, O. H.; Rosebrough, N. J.; Farr, A. L.; Randall, R. J. *J. Biol. Chem.* **1951**, *193*, 265−275.
(29) Dutton, P. L. *Methods Enzymol.* **1978**, *54*, 411−435.
(30) Johnson, M. K. In *Metal Clusters in Proteins*; Que, L., Jr., Ed.; ACS Symposium Series Vol. 372; American Chemical Society: Washington, DC, 1988; pp 326−342.

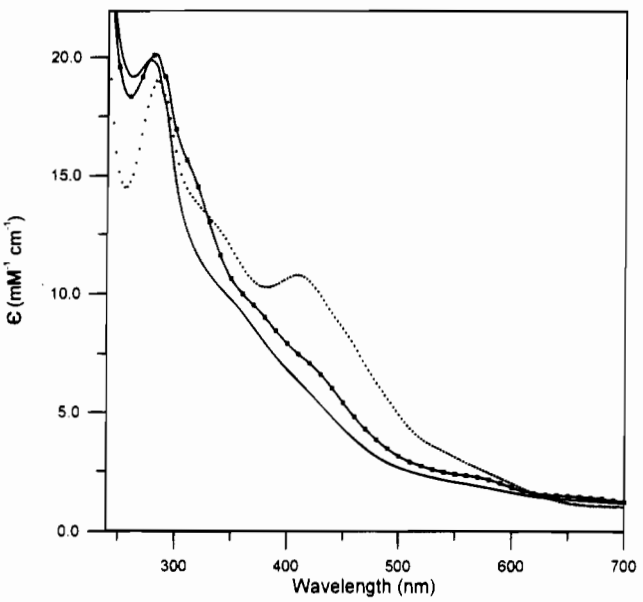

Figure 1. Effect of Mn^{2+} on the room-temperature absorption spectra of *P. furiosus* $[Fe_3S_4]$ Fd. The dotted line is the spectrum of Fd containing a $[Fe_3S_4]^+$ cluster, 400 μM in 100 mM Mes buffer, pH 6.3. The solid line with squares is the spectrum of the Fd containing a $[Fe_3S_4]^0$ cluster obtained by anaerobic addition of a 5-fold stoichiometric excess of sodium dithionite to the $[Fe_3S_4]^+$ form. The solid line is after anaerobic addition of a 10-fold stoichiometric excess of $Mn(OOCCH_3)_2$ to the $[Fe_3S_4]^0$ form.

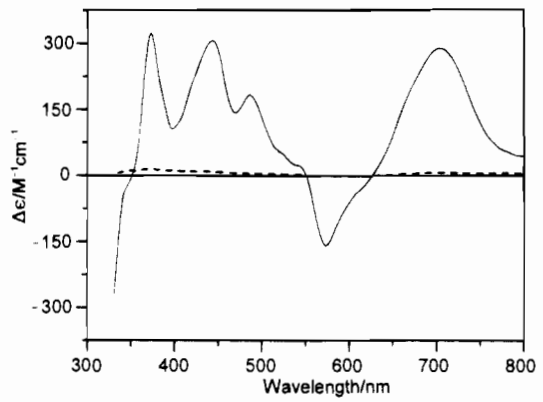

Figure 2. Effect of Mn^{2+} on the VTMCD spectrum of the $[Fe_3S_4]^0$ cluster in dithionite-reduced *P. furiosus* Fd. The solid line is the VTMCD spectrum of the $[Fe_3S_4]^0$ cluster prior to addition of Mn^{2+}, and the dashed line is after addition of a 10-fold stoichiometric excess of Mn^{2+}. The MCD spectra were recorded with a magnetic field of 4.5 T at 4.2 K. The sample was 600 μM in Fd, and the medium was 50 mM Tris/HCl buffer, pH 7.8, with 1 mM sodium dithionite and 55% (v/v) glycerol.

cluster in the presence of excess dithionite results in significant bleaching of the visible absorption; see Figure 1. Oxidation and removal of Mn^{2+} by aerobic gel filtration results in complete restoration of the $[Fe_3S_4]^+$ cluster as judged by the absorption and quantitative EPR studies. Since the visible absorption is associated primarily with S → Fe(III) charge transfer transitions, the bleaching indicates further reduction of the $[Fe_3S_4]^0$ fragment in the presence of Mn^{2+}. This observation supports the formation of a $[MnFe_3S_4]^+$ cluster, since incorporation of a divalent metal ion such as Zn^{2+}, Cd^{2+}, Co^{2+}, or Ni^{2+} is frequently accompanied by a further one-electron reduction in the presence of excess dithionite to yield $[MFe_3S_4]^+$ clusters.[8]

The effects of Mn^{2+} addition on the properties of the $[Fe_3S_4]^0$ Fd are much more dramatic in VTMCD studies; see Figure 2. Paramagnetic Fe−S clusters invariably exhibit temperature-dependent MCD spectra with numerous bands throughout the UV/visible region.[30,31] In accord with this, the $[Fe_3S_4]^0$ Fd exhibits an intense temperature-dependent MCD spectrum, and magnetization studies at discrete wavelengths are indicative of an $S = 2$ ground state with the axial zero-field splitting parameter, D, <0.[20] This spectrum is completely abolished on addition of Mn^{2+} in the presence of excess dithionite, and the resulting sample exhibits very weak, temperature-independent MCD. Likewise the addition of Mn^{2+} resulted in complete loss of the "$g = 10$" EPR signal that is characteristic of the $S = 2$ $[Fe_3S_4]^0$ cluster in *P. furiosus* Fd.[20] For temperatures in the range 4−70 K, no resonances were observed in perpendicular or parallel mode X-band EPR studies of Mn^{2+}-treated Fd containing $[Fe_3S_4]^0$ clusters. The characteristic six-line resonance of Mn^{2+} was observed in the spectra of samples prior to the removal of excess Mn^{2+} by incubation with EDTA followed by gel filtration (data not shown). Taken together, the EPR, VTMCD, and absorption results provide convincing evidence for the formation of a diamagnetic ($S = 0$) $[MnFe_3S_4]^+$ cluster in *P. furiosus* Fd.

Attempts to oxidize the $[MnFe_3S_4]^+$ Fd with retention of Mn were unsuccessful. Oxidation with stoichiometric amounts of thionin or ferricyanide, even in the presence of a 100-fold excess of Mn^{2+}, resulted samples containing a mixture of $S = {}^1/_2$ $[Fe_3S_4]^+$ and $S = 2$ $[Fe_3S_4]^0$ clusters as judged by EPR and VTMCD studies. Dye-mediated EPR redox titrations in the absence of excess Mn^{2+} showed no EPR signals for potentials in the range −450 to −100 mV. Above −100 mV, the characteristic $g = 2.02$ resonance of the $[Fe_3S_4]^+$ cluster was observed with an intensity that increased with increasing potential.

$[CoFe_3S_4]^+$ Clusters in *P. furiosus* Fd. Addition of Co^{2+} to samples of *P. furiosus* Fd containing $[Fe_3S_4]^0$ clusters, in the presence of excess dithionite, results in a slight bleaching of the visible absorption, analogous to that observed for the addition of Mn^{2+}; see Figure 1. The properties of the putative $[CoFe_3S_4]^+$ Fd prepared in this way were investigated by EPR and VTMCD spectroscopies. X-band EPR studies revealed no evidence of any resonance using either a parallel or perpendicular mode configuration over the range 0−600 mT with temperatures in the range 4−70 K and microwave powers up to 50 mW (data not shown). This result was obtained irrespective of the presence of 50% (v/v) glycerol, which is required for low-temperature MCD studies. The complete loss of the "$g = 10$" feature that is characteristic of the $S = 2$ ground state of the $[Fe_3S_4]^0$ cluster and the absence of the characteristic $S = {}^1/_2$ resonance of the $[CoFe_3S_4]^{2+}$ cluster[12,32,33] suggest complete conversion to a $[CoFe_3S_4]^+$ cluster. However, still open is the question of the spin state of this cluster since both diamagnetic ($S = 0$) and integer-spin paramagnetic ($S \geq 1$) ground states can be responsible for the complete absence of parallel and perpendicular mode EPR signals.

VTMCD spectroscopy provides a convenient method for distinguishing between these possibilities and determining the spin state of the $[CoFe_3S_4]^+$ cluster in *P. furiosus* Fd. VTMCD spectra recorded at temperatures between 1.69 and 54 K are shown in the top panel of Figure 3. The observation of temperature-dependent MCD bands throughout the UV/visible region shows that the cluster is paramagnetic. While detailed assignments of the electronic transitions responsible for the positive and negative MCD bands are not yet available, the

(31) Johnson, M. K.; Robinson, A. E.; Thomson, A. J. In *Iron-Sulfur Proteins*; Spiro, T. G., Ed.; Wiley: New York, 1982; pp 367−406.
(32) Zhou, J.; Scott, M. J.; Hu, Z.; Peng, G.; Münck, E.; Holm, R. H. *J. Am. Chem. Soc.* **1992**, *114*, 10843−10854.
(33) Roth, E. K. H.; Greneche, J. M.; Jordanov, J. *J. Chem. Soc., Chem. Commun.* **1991**, 105−107.

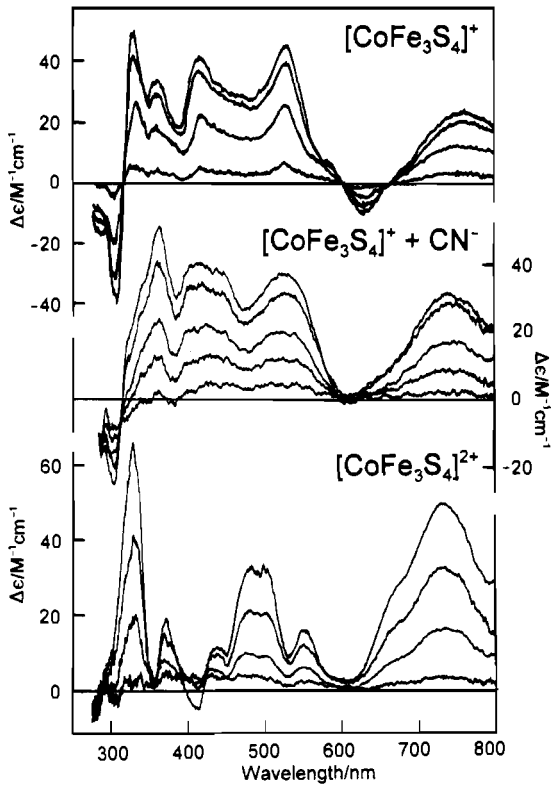

Figure 3. VTMCD spectra of *P. furiosus* [$CoFe_3S_4$] Fd. Top panel: $[CoFe_3S_4]^+$ cluster in dithionite-reduced Fd. The sample was 190 μM in Fd, and the medium was 50 mM Tris/HCl buffer, pH 7.8, with 2 mM sodium dithionite and 55%(v/v) glycerol. The spectra were recorded at 1.69, 4.22, 10.7, and 54 K. Middle panel: Cyanide-treated $[CoFe_3S_4]^+$ cluster in dithionite-reduced Fd. The sample was the same as described in the top panel except that the final solution was 50 mM in potassium cyanide. The spectra were recorded at 1.70, 4.22, 9.4, 19, and 53 K. Bottom panel: $[CoFe_3S_4]^{2+}$ cluster in thionin-oxidized Fd. The sample was the same as that described in the top panel except that it was oxidized using a minimal volume of a concentrated thionin solution. The spectra were recorded at 1.66, 4.22, 10.1, and 53 K. For all three samples the spectra were recorded with an applied magnetic field of 4.5 T and all MCD bands increase in intensity with decreasing temperature.

pattern of bands (i.e. signs and wavelengths) has been shown to provide a reliable indicator of cluster type (i.e. $[Fe_2S_2]$, linear and cubane $[Fe_3S_4]$, cubane $[Fe_4S_4]$, or double-cubane $[Fe_8S_8]$ clusters).[20,30,31,34-36] Hence, it is not surprising the VTMCD spectra of the $[CoFe_3S_4]^+$ cluster in *P. furiosus* Fd bear a striking resemblance to those reported previously for $S = {}^3/_2$ and ${}^1/_2$ $[Fe_4S_4]^+$ clusters in synthetic compounds and a wide range of proteins.[20,30,31,34]

MCD magnetization studies in which the MCD intensity at a fixed wavelength is monitored as a function of increasing magnetic field at fixed temperature provide a means of assessing the properties of the ground state from which the electronic transition originates.[30,31,37-40] MCD magnetization data for the $[CoFe_3S_4]^+$ Fd were collected at 526 nm at 1.69, 4.22, 10.3, 23, 54, and 95 K and are shown in the top panel of Figure 4 plotted as MCD intensity as a function of $\beta B/2kT$, where β is the Bohr magneton, B is the magnetic flux, k is Boltzmann's constant, and T is the absolute temperature (the data at the three

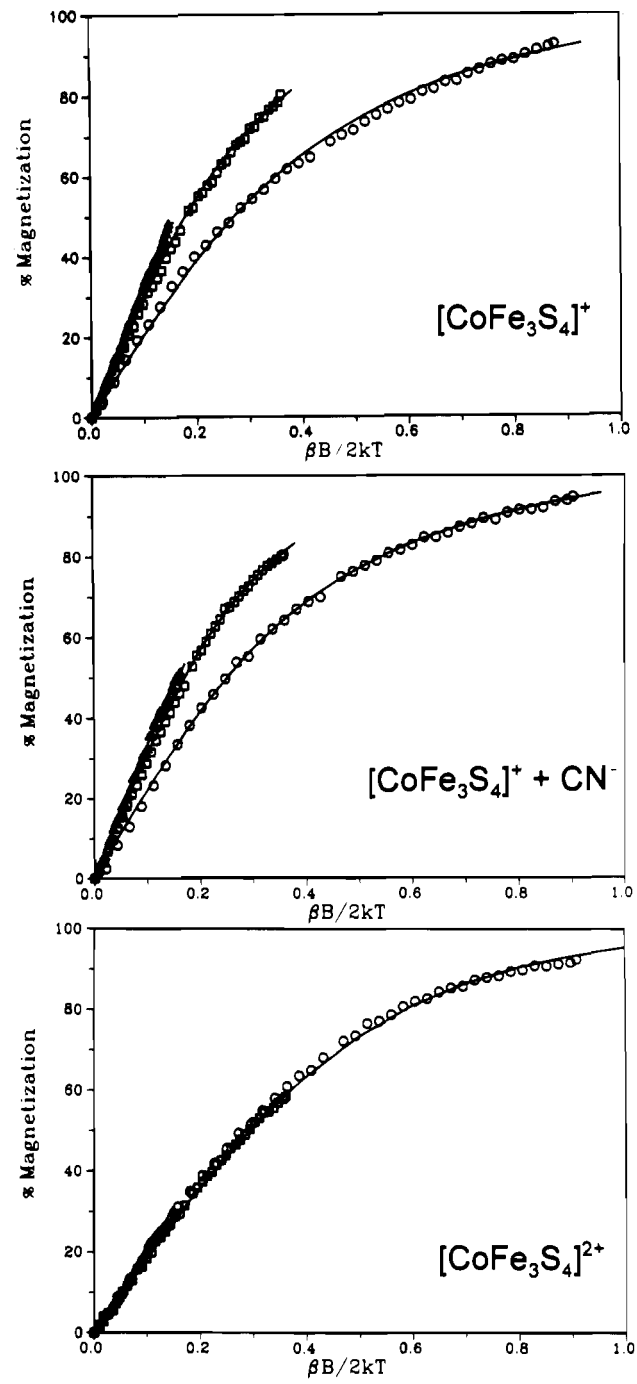

Figure 4. MCD magnetization data for *P. furiosus* [$CoFe_3S_4$] Fd. Top panel: $[CoFe_3S_4]^+$ cluster in dithionite-reduced Fd. Magnetization data were collected at 526 nm with magnetic fields between 0 and 4.5 T at fixed temperatures of 1.69 K (○), 4.22 K (□), and 10.3 K (△). The solid lines are theoretical magnetization curves, computed using eq 6 of ref 39, for an *xy*-polarized transition originating from an isolated "doublet" ground state with $g_{\|} = 4.2$, $g_{\perp} = 0.0$, and $\delta = 3.6$ cm^{-1}. Middle panel: Cyanide-treated $[CoFe_3S_4]^+$ cluster in dithionite-reduced Fd. Magnetization data were collected at 523 nm with magnetic fields between 0 and 4.5 T at fixed temperatures of 1.70 K (○), 4.22 K (□), and 9.4 K (△). The solid lines are theoretical magnetization curves, computed using eq 6 of ref 39, for an *xy*-polarized transition originating from an isolated "doublet" ground state with $g_{\|} = 4.3$, $g_{\perp} = 0.0$, and $\delta = 3.3$ cm^{-1}. Bottom panel: $[CoFe_3S_4]^{2+}$ cluster in thionin-oxidized Fd. Magnetization data were collected at 735 nm with magnetic fields between 0 and 4.5 T at fixed temperatures of 1.66 K (○), 4.22 K (□), and 10.1 K (△). The solid line is theoretical magnetization data, computed using eq 1 of ref 40, for a transition originating from an isolated $S = {}^1/_2$ doublet ground state with $g_{\|} = 1.94$, $g_{\perp} = 1.86$, and $m_z/m_{xy} = -0.2$. The sample conditions are described in the caption of Figure 3.

(34) Onate, Y. A.; Finnegan, M. G.; Hales, B. J.; Johnson, M. K. *Biochim. Biophys. Acta* **1993**, *1164*, 113-123.
(35) Fu, W.; Drozdzewski, P. M.; Davies, M. D.; Sligar, S. G.; Johnson, M. K. *J. Biol. Chem.* **1992**, *267*, 15502-15510.
(36) Richards, A. J. M.; Thomson, A. J.; Holm, R. H.; Hagen, K. S. *Spectrochim. Acta* **1990**, *46A*, 987-993.
(37) Thomson, A. J.; Johnson, M. K. *Biochem. J.* **1980**, *191*, 411-420.

highest temperatures have been omitted for clarity). The observation that the magnetization data are "nested" (i.e., plots obtained at different temperatures do not overlap) dictates that the transitions originate from a ground state with $S > {}^1/_2$ that is subject to zero-field splitting. A clearer separation of field and temperature effects is obtained by replotting the data in terms of the temperature dependence of the MCD intensity at fixed applied fields (data not shown). Such a plot shows that the saturation limit is field dependent, which necessitates a substantial field-induced mixing (*B* term) contribution to the MCD intensity. This *B* term contribution is clearly temperature dependent as a result of thermal population of the mixing state(s) over the temperature range of the experiment. A *C* term contribution is also indicated by the tendency toward magnetic saturation as a function of increasing magnetic field at a fixed temperature of 1.69 K.

Magnetization behavior arising from overlapping temperature-dependent *B* and *C* terms is commonly observed for non-Kramers doublet states which are split in zero field by a rhombic splitting.[38] Consequently, the data were fit to an expression derived by Whittaker and Solomon[39] to analyze MCD magnetization data arising from a non-Kramers doublet that is subject to rhombic zero-field splitting, δ. This analysis assumes a purely *x,y*-polarized transition from a randomly oriented chromophore with $g_{\|} \neq 0$ and $g_{\perp} = 0$ and that the *B* term component arises exclusively from field-induced mixing within the non-Kramers doublet (i.e. a temperature-dependent *B* term). The best fit parameters were $g_{\|} = 4.2$ and $\delta = 3.6$ cm^{-1}, and the theoretical plots constructed for these parameters are in excellent agreement with the experimental data; see Figure 4. An effective $g_{\|}$ value close to 4.0 is consistent with $S = 1$ spin Hamiltonian behavior for a spin-only value for $g_0 = 2.00$. Hence, MCD magnetization studies are consistent with a rhombic $S = 1$ ground state with a negative axial zero-field splitting parameter, *D*, leaving a rhombically split $M_s = \pm 1$ "doublet" lowest in energy. These ground state properties are in accord with the absence of X-band EPR signals in parallel or perpendicular mode, since the zero-field splitting within the ground state doublet is an order of magnitude greater than the microwave energy.

The combination of EPR, ENDOR, VTMCD, and/or Mössbauer studies has demonstrated that the unique metal sites of the $[Fe_4S_4]^+$ and $[NiFe_3S_4]^+$ clusters in *P. furiosus* Fd are capable of binding exogenous ligands such as cyanide.[11,14,23,25] A similar approach using the combination of EPR and VTMCD was used to investigate the possibility of cyanide binding to the $[CoFe_3S_4]^+$ cluster. The addition of a 250-fold excess of potassium cyanide did not elicit an X-band EPR signal in parallel or perpendicular mode, but it did produce a marked change in the VTMCD spectrum; see Figure 3. While the overall form of the spectrum is still characteristic of a $[Fe_4S_4]^+$ cluster, cyanide addition induces changes in the bandwidth and relative intensities of the MCD bands and loss of the negative band centered at 620 nm. Moreover, these changes are completely reversible, since the spectrum reverts to its original form on removal of cyanide by anaerobic gel filtration. Subsequent VTMCD studies with smaller and larger excesses of cyanide revealed that the changes are complete with a 100-fold stoichiometric excess of cyanide. MCD magnetization studies indicate that cyanide addition induces only minor changes in the ground state properties of the $[CoFe_3S_4]^+$ cluster. The data collected at 523 nm are shown in Figure 4. Analysis using the procedure outlined above gave best fit parameters $g_{\|} = 4.3$ and $\delta = 3.3$ cm^{-1}, compared to $g_{\|} = 4.2$ and $\delta = 3.6$ cm^{-1} in the absence of cyanide.

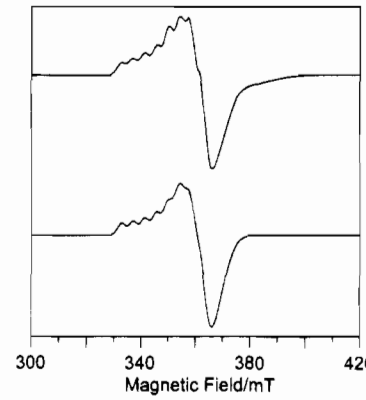

Figure 5. X-band EPR spectra of the $[CoFe_3S_4]^{2+}$ cluster in thionin-oxidized *P. furiosus* Fd. (a) Upper curve: EPR spectrum recorded at 10 K; microwave power, 10 mW; microwave frequency, 9.44 GHz; modulation amplitude, 0.63 mT. (b) Lower curve: Simulation with $g_{x,y,z} = 1.862, 1.865, 1.937$, $a_{x,y,z} = 0.0, 0.0, 4.3$ mT, and linewidths of 11.0, 8.5, and 2.8 mT, respectively. The sample is as described in the caption of Figure 3.

$[CoFe_3S_4]^{2+}$ Clusters in *P. furiosus* Fd. Anaerobic oxidation of the $[CoFe_3S_4]^+$ cluster was carried out by the addition of a stoichiometric amount of thionin in the presence of a 10-fold stoichiometric excess of Co^{2+}. The resulting EPR spectrum is shown in Figure 5. The spectrum, which is similar to, albeit more axial than, that reported for the $[CoFe_3S_4]^{2+}$ cluster in *D. gigas* FdII[12] and the structurally characterized synthetic clusters $[CoFe_3S_4(Smes)_4]^{2-}$ and $[CoFe_3S_4(Stib)_4]^{2-}$,[32,33] arises from an approximately axial $S = {}^1/_2$ species with the low-field component split into eight well-resolved lines as a result of hyperfine interaction with a single ^{59}Co ($I = {}^7/_2$) nucleus. The spectrum can be simulated to a good approximation by a powder simulation with $g_{x,y,z} = 1.862, 1.865, 1.937$ and $a_{x,y,z} = 0.0, 0.0, 4.3$ mT, with line widths of 11.0, 8.5, and 2.8 mT, respectively; see Figure 5. Spin quantitations of this resonance at temperatures in the range 10−30 K for three different samples indicate that it accounts for 0.8 ± 0.2 spin/molecule. EPR studies at lower temperatures and high microwave powers (e.g. 10 K and 50 mW) gave no evidence for the presence of $S = {}^1/_2$ $[Fe_3S_4]^+$ clusters. Such clusters exhibit fast-relaxing EPR signals with a sharp positive feature centered at $g = 2.02$.[20] However, EPR studies showed that $[Fe_3S_4]^+$ clusters were readily formed via oxidative degradation of the $[CoFe_3S_4]^{2+}$ cluster when excess oxidant was used or the oxidation was carried out without excess Co^{2+}.

VTMCD spectra of samples containing exclusively $[CoFe_3S_4]^{2+}$ clusters, as judged by parallel quantitative EPR studies, are shown in Figure 3, bottom panel. While the observation of temperature-dependent MCD bands throughout the UV/visible region shows the presence of a paramagnetic Fe−S center, cursory inspection of the temperature dependence behavior reveals that the ground state is quite different from that of the $[CoFe_3S_4]^+$ cluster. Indeed, MCD magnetization data, collected at 735 nm, are well fit at all temperatures by theoretical data constructed for the *g* values of the EPR-detectable $S = {}^1/_2$ species; see Figure 4. The observed MCD bands therefore originate from the $S = {}^1/_2$ ground state that is responsible for the EPR signal. The VTMCD spectra are quite distinct from those observed for $S = {}^1/_2$ $[Fe_3S_4]^+$ or $S = 1$ $[CoFe_3S_4]^+$ clusters in *P. furiosus* but are very similar in form to those reported recently for the $S = 2$ $[TlFe_3S_4]^+$ cluster.[18] This is consistent

(38) Johnson, M. K. In *Physical Methods in Inorganic and Bioinorganic Chemistry*; Que, L., Jr., Ed.; University Science Books, in press.
(39) Whittaker, J. W.; Solomon, E. I. *J. Am. Chem. Soc.* **1988**, *110*, 5329–5339.

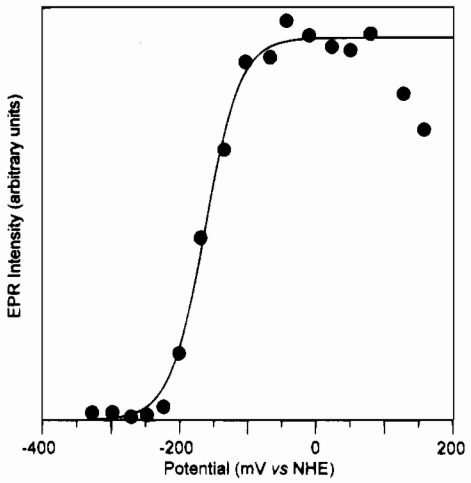

Figure 6. EPR-monitored dye-mediated redox titration for the $[CoFe_3S_4]^{2+,+}$ cluster in *P. furiosus* Fd. EPR intensity corresponds to the peak-to-trough intensity of the derivative feature centered at g = 1.86 of the $[CoFe_3S_4]^{2+}$ species, measured at 10 K with 1-mW microwave power. The solid line is the best fit to a one-electron Nernst plot with a midpoint potential of −163 mV *vs* NHE (pH 7.6). The experimental protocol is described under Materials and Methods.

with a formalism in which $[Fe_3S_4]^0$ clusters are coordinated to Tl^+ or Co^{2+} via the three μ_2-S atoms. In both cases, the intense positive MCD bands at ~320 nm, which are not present in the VTMCD spectra of $S = 2$ $[Fe_3S_4]^0$ or $[ZnFe_3S_4]^{2+}$ clusters (see below), are tentatively attributed to charge transfer transitions localized on Tl^+ or Co^{2+}.

The midpoint potential of the $[CoFe_3S_4]^{2+,+}$ couple was assessed by dye-mediated oxidative titrations, using ferricyanide as oxidant, in which the intensity of the $S = {}^1/_2$ $[CoFe_3S_4]^{2+}$ EPR signal was monitored as a function of potential; see Figure 6. In the range −350 to +100 mV (*vs* NHE), the data are well fit by a one-electron Nernst plot with a midpoint potential of −163 ± 10 mV *vs* NHE (pH 7.5). At 0 mV, a weak "g = 2.02" resonance that is characteristic of the $[Fe_3S_4]^+$ cluster was apparent, suggesting oxidative degradation of the heterometallic cluster via removal of the Co(II). This resonance becomes progressively larger with increasing potential and presumably accounts for the observed decrease in the intensity of the $[CoFe_3S_4]^{2+}$ EPR signal at potentials above +100 mV.

Attempts to bind cyanide to the $[CoFe_3S_4]^{2+}$ cluster were unsuccessful. Cyanide selectively removed Co from the cluster to give samples containing a mixture of $S = 2$ $[Fe_3S_4]^0$ and $S = {}^1/_2$ $[Fe_3S_4]^+$ clusters, as judged by parallel VTMCD and EPR studies. Such behavior is consistent with cyanide binding exclusively at the unique metal site and is in accord with previous work on heteronuclear cubanes which indicates that the affinity of an $[Fe_3S_4]$ cluster for exogenous metal ions decreases as the oxidation state of the Fe−S fragment increases.[10,17]

$[ZnFe_3S_4]^+$ Clusters in *P. furiosus* Fd. Addition of a 10-fold excess of Zn^{2+} to the $[Fe_3S_4]^0$ form of *P. furiosus* Fd in the presence of excess sodium dithionite resulted in changes in the visible absorption identical to those observed for addition of Co^{2+} or Mn^{2+}; See Figure 1. The EPR spectra of the resulting samples were invariant to pH over the range 6−11 (see Figure 7a) and are very similar to those of the ^{57}Fe-enriched samples of *P. furiosus* Fd containing $[ZnFe_3S_4]^+$ clusters that were used for Mössbauer analysis,[11] except for substantially improved resolution of the low-field components; see Figure 8. The spectra reported here for the as prepared $[ZnFe_3S_4]^+$ cluster are readily interpreted as a mixture of two $S = {}^5/_2$ species, and the effective g values of both can be rationalized using an

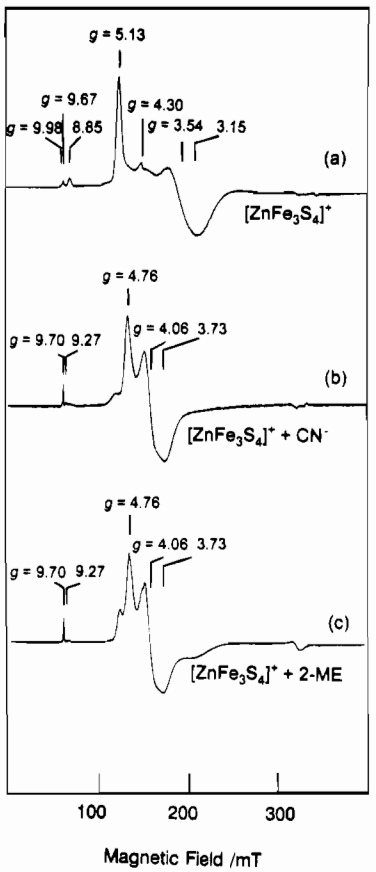

Figure 7. X-band EPR spectra of the $[ZnFe_3S_4]^+$ cluster in dithionite-reduced *P. furiosus* Fd. The samples are as prepared (a), after addition of a 50-fold excess of cyanide (b), and after addition of a 250-fold excess of 2-mercaptoethanol (c). All sample concentrations were 0.35 mM in 100 mM CAPS/NaOH buffer, pH 10.5. Spectra were recorded at 7.5 K; microwave power, 10 mW; microwave frequency, 9.43 GHz; modulation amplitude, 0.63 mT.

isotropic $S = {}^5/_2$ spin Hamiltonian:

$$\mathcal{H} = g_0\beta\mathbf{H}\cdot\mathbf{S} + D(\mathbf{S}_z^2 - S(S+1)/3) + E(\mathbf{S}_x^2 - \mathbf{S}_y^2) \quad (1)$$

The major species is responsible for the absorption-shaped features centered at g = 9.98 and 8.85 and the dominant component with a near-axial line shape at $g_{x,y,z}$ = 5.13, 3.54, 3.15. On the basis of their temperature-dependence behavior (see Figure 8), the g = 9.98 and 8.85 features are attributed to the low-field components of resonances from the lower and upper doublets, respectively, with the middle doublet responsible for the dominant "axial" species. For example, for $D < 0$, E/D = 0.18, and $g_0 = 2$, eq 1 predicts $g_{x,y,z}$ = (0.23, 0.20, 9.92), (3.51, 3.16, 5.19), and (2.25, 8.95, 1.27) for the lower, middle, and upper doublets, respectively, in good agreement with the observed values. The energy separation between the lower and upper zero-field doublets, Δ, can be estimated from the slope of a plot of the logarithm of the ratio of the intensity of the two field resonances ($\log(I_{g=9.98}/I_{g=8.85})$) versus the reciprocal of the absolute temperature, which is a straight line within experimental error of the measurement of the absolute temperature (not shown). This leads to Δ = 15 ± 3 cm^{-1}, which corresponds to $D = -2.3 \pm 0.5$ cm^{-1}. A similar, albeit more rhombic, $S = {}^5/_2$ ground state (E/D = 0.25, $D = -2.7 \pm 0.5$ cm^{-1}) has been reported for the $[ZnFe_3S_4]^+$ cluster in *D. gigas* FdII.[9]

The minor species is responsible for the absorption-shaped band at g = 9.67, and possibly some of the derivative-shaped resonances at g = 4.30. These resonances are generally the only observable features of a rhombic (E/D = 0.33) $S = {}^5/_2$

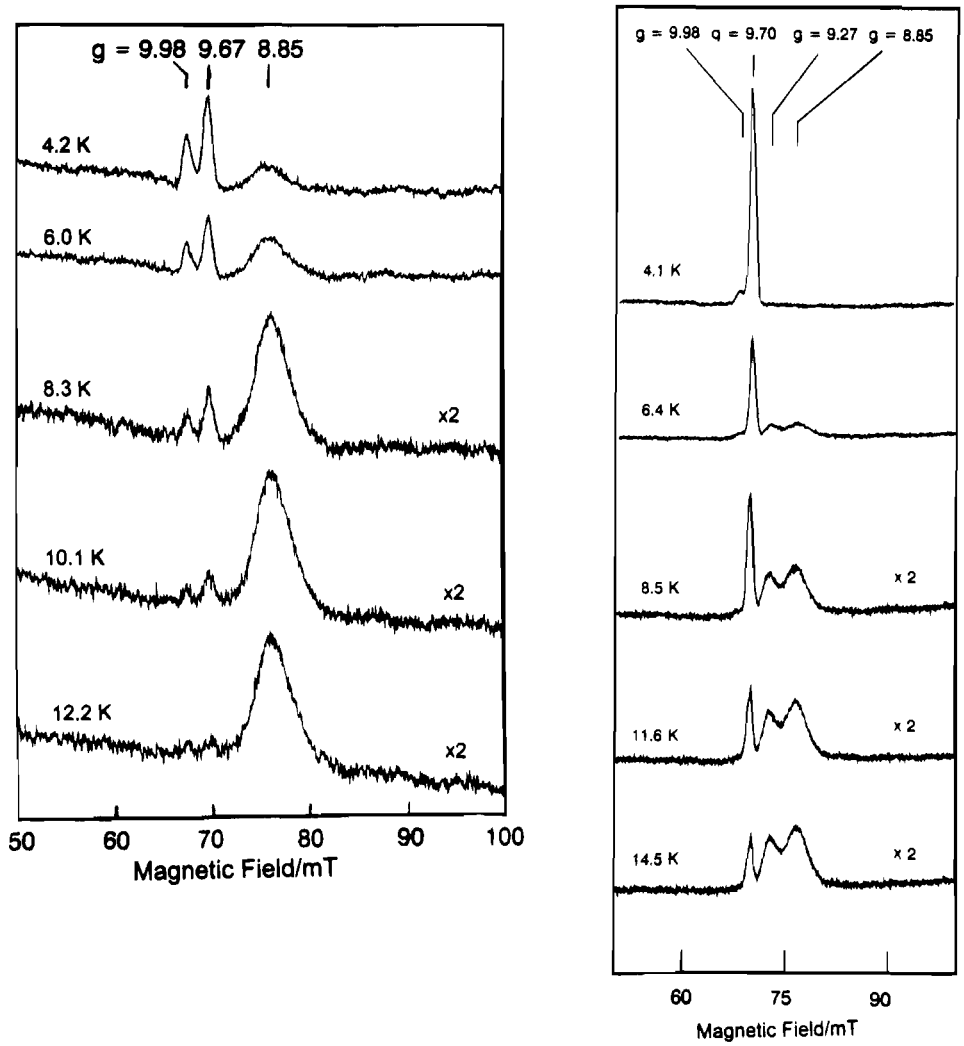

Figure 8. Temperature dependence of the low-field EPR spectrum of the $[ZnFe_3S_4]^+$ cluster in dithionite-reduced *P. furiosus* Fd. Left panel: As prepared. Spectra were recorded with a microwave power of 50 mW and at the indicated temperatures. Right panel: After addition of a 250-fold excess of 2-mercaptoethanol. Spectra were recorded with a microwave power of 20 mW and at the indicated temperatures. The samples and all other conditions of measurement are the same as for Figure 7. Multiplication factors indicate relative gains.

ground state which is predicted to have $g_{x,y,z}$ = (0.86, 0.61, 9.68), (4.29, 4.29, 4.29), and (0.86, 9.68, 0.61) for the lower, middle, and upper doublets, respectively, for $g_0 = 2$. However, the relative intensities as a function of temperature of the observed $g = 4.30$ and 9.67 species are inconsistent with both arising from the same $S = {}^5/_2$ ground state. A more likely explanation is that the $g = 9.67$ resonance arises from the minor species which has $|D| > 5$ cm^{-1} such that the middle doublet is not sufficiently populated over the temperature range of the EPR measurements and that the observed $g = 4.30$ resonance arises for the most part from an impurity in the quartz cryostat. The quartz cryostat exhibits a weak feature at $g = 4.30$ with similar intensity under comparable conditions. On the basis of this interpretation and considering the relative intensities and transition probabilities for the $g = 9.98$ and 9.68 features, the minor species is estimated to account for 10% of the major $S = {}^5/_2$ species.

VTMCD spectra in the UV/visible/near-IR region recorded at 4.5 T for temperatures in the range 1.64−50 K are shown in Figure 9. Identical spectra were obtained for samples in 100 mM Mes buffer (pH 5.9), 100 mM EPPS buffer (pH 7.8), and 100 mM CAPS/NaOH (pH 10.5). Similar spectra that differ in the relative intensities but show a 1:1 correspondence in the frequency and sign of each temperature-dependent MCD band are observed for the $[ZnFe_3S_4]^+$ cluster in *D. gigas* FdII; see

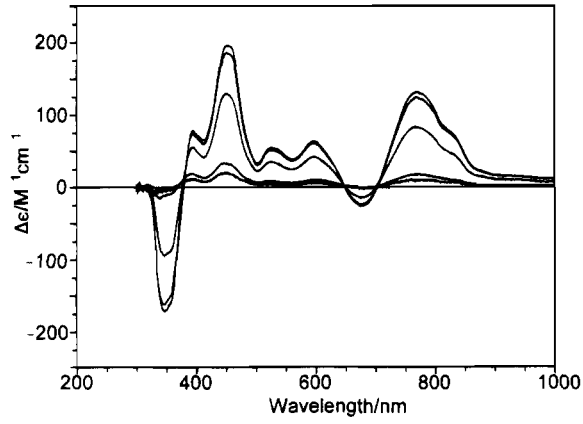

Figure 9. VTMCD spectra of the $[ZnFe_3S_4]^+$ cluster in dithionite-reduced *P. furiosus* Fd. MCD spectra were recorded with a magnetic field of 4.5 T at temperatures of 1.64, 4.22, 10.2, 20.2, and 50.1 K. The intensities of all transitions increase with decreasing temperature. The final solution was 0.20 mM in Fd, and the medium was 50 mM Tris/HCl buffer, pH 7.8, with 2 mM dithionite and 55% (v/v) ethylene glycol.

Figure 10. Hence it can be concluded that $[ZnFe_3S_4]^+$ clusters give rise to characteristic low-temperature MCD spectra consisting of broad positive bands centered between 850−760 and 1500−1000 nm, multiple positive bands in the region between

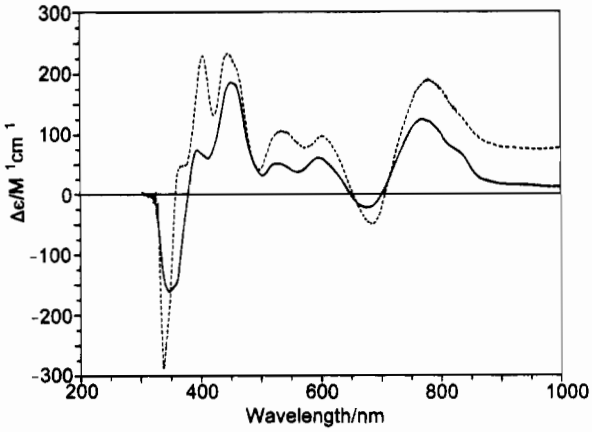

Figure 10. Comparison of the low-temperature MCD spectra of $[ZnFe_3S_4]^+$ clusters in *D. gigas* FdII (broken line) and *P. furiosus* Fd (solid line). The spectra were recorded at 4.5 T and 4.2 K. The *P. furiosus* Fd sample is as described in the caption of Figure 9. The *D. gigas* FdII sample was 0.32 mM in Fd, and the medium was 50 mM Tris/HCl buffer, pH 7.6, with 2 mM dithionite and 50% (v/v) glycerol.

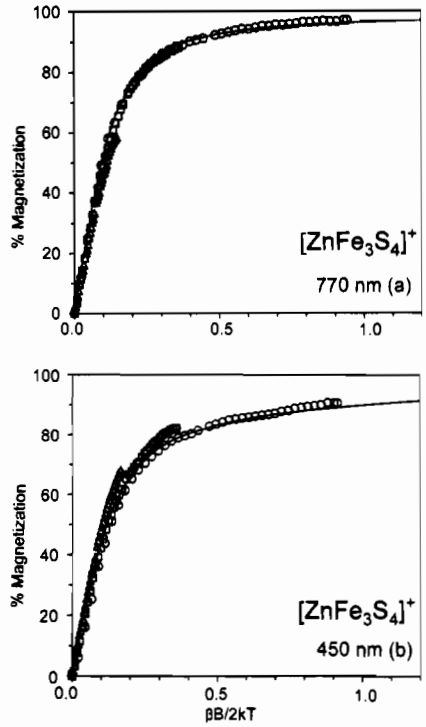

Figure 11. MCD magnetization plots for the $[ZnFe_3S_4]^+$ cluster in dithionite-reduced *P. furiosus* Fd. Sample conditions are described in the caption of Figure 10. MCD magnetization was done at 770 nm (a) and 450 nm (b). Temperatures: ○, 1.64 K; □, 4.22 K; △, 10.2 K. Magnetic fields were between 0 and 4.5 T. Solid lines are theoretical magnetization curves, constructed using eq 1 of ref 40, for transitions from an isolated doublet ground state with $g_{\parallel} = 9.9$, $g_{\perp} = 0.22$, and a polarization ratio $m_z/m_{xy} = -0.4$ (a) and with $g_{\parallel} = 9.9$, $g_{\perp} = 0.22$, and a polarization ratio $m_z/m_{xy} = -1.4$ (b).

400 and 650 nm, and pronounced negative features between 650−700 and 250−400 nm.

The $S = {}^5/_2$ ground state of the $[ZnFe_3S_4]^+$ cluster in *P. furiosus* Fd is also manifest in MCD magnetization data collected at 770 nm and 450 nm; see Figure 11. The nested set of plots is a consequence of the Boltzmann population and/or field-induced mixing of zero-field components of the $S = {}^5/_2$ ground state.[38−40] At the lowest temperature (1.64 K), the data can be simulated to a good approximation by theoretical data constructed using the effective g values of the lowest doublet of the zero-field-split manifold assuming only C term contribution and allowing the transition polarization to vary. This analysis suggests a significant difference in transition polarization at these wavelengths, with the 450-nm band having a significant z-polarized component, i.e. $m_z/m_{xy} = -0.4$ at 770 nm compared to -1.4 at 450 nm.

The ability of the $[ZnFe_3S_4]^+$ cluster in *P. furiosus* Fd to bind exogenous ligands such as thiolates and cyanide was assessed by investigating the effects of excess 2-mercaptoethanol and cyanide on the EPR and VTMCD properties. Figure 7 shows EPR evidence for exogenous ligand binding to the $[ZnFe_3S_4]^+$ cluster. The addition of a 250-fold excess of 2-mercaptoethanol (100 mM CAPS/NaOH, pH 10.5) produces new absorption-shape features at $g = 9.70$ and 9.27 and a dominant component with a rhombic line shape, $g_{x,y,z} = 4.76, 4.06, 3.73$; See Figure 7c. Analogous features were also apparent in spectra of samples treated with a 50-fold excess of potassium cyanide at both pH 10.5 (100 mM CAPS/NaOH) and pH 7.8 (50 mM Tris/HCl); see Figure 7b. Parallel studies in the absence of cyanide or thiolate as a function of pH showed that the changes in the EPR spectra are not a result of alkaline pH. Moreover, the changes in the EPR are fully reversible, since the spectra revert to that of the unligated form after anaerobic gel filtration to remove the excess ligand. The weaker resonances at $g = 5.12$, 9.98, and 8.85 correspond to those of the $S = {}^5/_2$ $[ZnFe_3S_4]^+$ cluster in dithionite-reduced *P. furiosus* Fd in the absence of exogenous ligands. Indeed the relative intensity of these features depends upon the concentration of the exogenous ligand. Hence these features are attributed to residual unligated clusters.

A detailed study of the temperature-dependence behavior of the low-field region of both the cyanide- and 2-mercaptoethanol-treated samples was carried out in order to assess the ground state spin-Hamiltonian parameters; see Figure 8. The relative intensity of the resonances at $g = 9.70$ and 9.27 are strongly temperature dependent, with $g = 9.70$ dominating the spectrum at low temperatures. The effective g-values and observed temperature dependence of the absorption-shaped features at $g = 9.70$ and $g = 9.27$ indicate that these resonances are from the lower and upper doublets, respectively, of a zero-field-split $S = {}^5/_2$ ground state. For $D < 0$, $E/D = 0.25$, and $g_0 = 1.99$, the spin Hamiltonian (eq 1) predicts $g_{x,y,z} = (0.47, 0.36, 9.79)$, (4.06, 3.74, 4.74), and (1.44, 9.35, 0.92) for the lower, middle, and upper doublets, respectively, in good agreement with the observed values. The energy separation between the lower and upper zero-field doublets, Δ, was again estimated from the slope of a plot of the logarithm of the ratio of the intensity of the two field resonances ($\log(I_{g=9.70}/I_{g=9.27})$) versus the reciprocal of the absolute temperature (not shown). Such plots yielded straight lines within the experimental error of the measurement of the absolute temperature for both the cyanide and 2-mercaptoethanol-treated samples, and the slopes indicate $\Delta = 17.6 \pm 3.0$ cm^{-1}, which corresponds to $D = -2.5 \pm 0.5$ cm^{-1} for the mercaptoethanol-bound $[ZnFe_3S_4]^+$ cluster, and $\Delta = 17.3 \pm 4.0$ cm^{-1}, which corresponds to $D = -2.5 \pm 0.6$ for the cyanide-bound $[ZnFe_3S_4]^+$ cluster. Of particular interest is that the ground state parameters for the thiolate-treated $[ZnFe_3S_4]^+$ cluster in *P. furiosus* Fd are very similar to those reported for the $[ZnFe_3S_4]^+$ cluster in *D. gigas* FdII, i.e. $E/D = 0.25$ and $D = -2.7 \pm 0.5$ cm^{-1}.[9]

VTMCD spectra recorded for the $[ZnFe_3S_4]^+$ cluster in *P. furiosus* Fd, with a 50-fold excess of potassium cyanide and 250-fold excess of 2-mercaptoethanol, are shown in Figure 12. For the cyanide-treated samples, identical spectra were observed

(40) Bennett, D. E.; Johnson, M. K. *Biochim. Biophys. Acta* **1987**, *911*, 71−80.

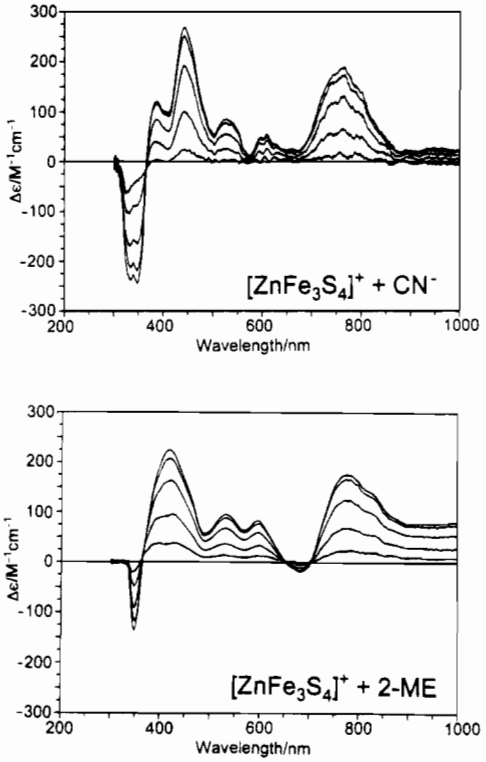

Figure 12. VTMCD spectra of the $[ZnFe_3S_4]^+$ cluster in dithionite-reduced *P. furiosus* Fd treated with exogenous ligands. Upper panel: Cyanide-treated MCD spectra recorded with a magnetic field of 4.5 T at temperatures of 1.60, 4.22, 9.43, 21.3, and 82.1 K. The intensities of all transitions increase with decreasing temperature. The sample was prepared by treating the reduced $[ZnFe_3S_4]^+$ form of *P. furiosus* Fd with a 10-fold stoichiometric excess of potassium cyanide. The final solution was 0.40 mM in Fd, and the medium was 50 mM Tris/HCl buffer, pH 7.8, with 2 mM dithionite and 55% (v/v) glycerol. Lower panel: 2-Mercaptoethanol-treated MCD spectra recorded with a magnetic field of 4.5 T at temperatures of 1.70, 4.22, 9.14, 19.4, and 53.1 K. The intensities of all transitions increase with decreasing temperature. The sample was prepared by treating the reduced $[ZnFe_3S_4]^+$ form of *P. furiosus* Fd with a 250-fold stoichiometric excess of 2-mercaptoethanol. The final solution was 0.32 mM in Fd, and the medium was 100 mM CAPS/NaOH buffer, pH 10.5, with 2 mM dithionite and 55% (v/v) glycerol.

for samples in 50 mM Tris/HCl buffer (pH 7.8) and in 100 mM CAPS/NaOH buffer (pH 10.5). Clearly, the electronic structure of the cluster is somewhat perturbed by cyanide or thiolate binding. However the pattern and sign of the MCD bands are preserved and the relative intensity of the bands for the mercaptoethanol-treated sample more closely resembles that of the $[ZnFe_3S_4]^+$ cluster in *D. gigas* FdII; *cf.* Figures 10 and 12. Magnetization data collected at 750 and 440 nm for the cyanide-treated $[ZnFe_3S_4]^+$ cluster and at 775 and 420 nm for the mercaptoethanol-treated $[ZnFe_3S_4]^+$ cluster (data not shown) are fully consistent with the EPR-determined ground state properties. In all cases, the lowest temperature data (1.66 K) were well fit by theoretical data constructed for a doublet with $g_{\parallel} = 9.7$ and $g_{\perp} = 0.4$, provided the polarization ratio was allowed to vary ($m_z/m_{xy} = -0.5$ at 775 nm and -0.8 at 420 nm for the mercaptoethanol-treated sample, and $m_z/m_{xy} = -0.8$ at 750 nm and -0.5 at 440 nm for the cyanide-treated sample). In summary, both the EPR and VTMCD results attest to reversible exogenous ligand binding at the Zn site and the properties of the thiolate-bound cluster lend support to the view that the Zn site is coordinated by the available cysteinate residue in *D. gigas* FdII.

$[ZnFe_3S_4]^{2+}$ Clusters in *P. furiosus* Fd. Initial attempts to oxidize the $[ZnFe_3S_4]^+$ cluster in *P. furiosus* Fd with retention

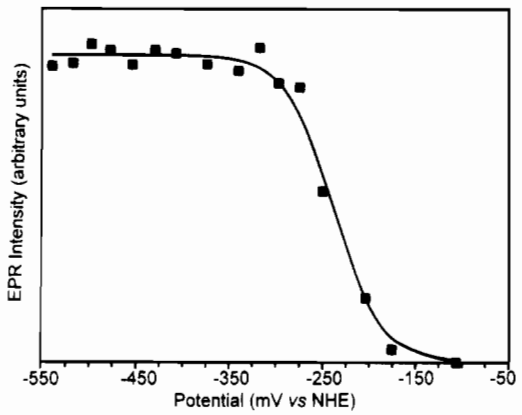

Figure 13. EPR-monitored, dye-mediated redox titration for the $[ZnFe_3S_4]^{2+,+}$ cluster in *P. furiosus* Fd. EPR intensity corresponds to the amplitude of the $g = 5.13$ component of the $[ZnFe_3S_4]^+$ species, measured at 10 K with 10-mW microwave power. The solid line is the best fits to a one-electron Nernst plot with a midpoint potential of -241 mV *vs* NHE (pH 7.6). The experimental protocol is described under Materials and Methods.

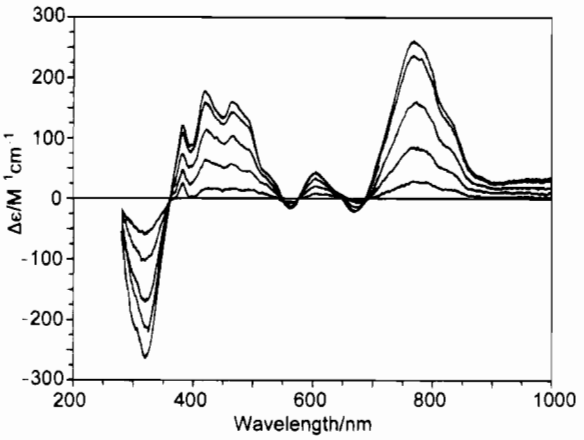

Figure 14. VTMCD spectra of the $[ZnFe_3S_4]^{2+}$ cluster in *P. furiosus* Fd. MCD spectra were recorded with a magnetic field of 4.5 T at temperatures of 1.64, 4.22, 9.6, 19.7, and 52.9 K. The intensities of all transitions increases with decreasing temperature. The sample was prepared by oxidizing the reduced $[ZnFe_3S_4]^+$ form of *P. furiosus* Fd with thionin and poising the potential at -197 mV *vs* NHE. The final solution was 0.40 mM in Fd, and the medium was 50 mM Tris/HCl buffer, pH 7.6, with 55% (v/v) ethylene glycol.

of the Zn^{2+} ion were only partially successful. Anaerobic oxidation with a 10-fold excess of ferricyanide resulted in >50% degradation to $[Fe_3S_4]^+$, as judged by quantitative EPR and VTMCD studies, even in the presence of excesses of Zn^{2+} up to 50-fold. Successful one-electron oxidation with minimal degradation was eventually accomplished under anaerobic conditions, after removal of excess Zn^{2+} and dithionite, using a stoichiometric amount of thionin. A dye-mediated redox titration in which the intensity of the $g = 5.13$ resonance of the $[ZnFe_3S_4]^+$ cluster was monitored as a function of potential during thionin oxidation is shown in Figure 13. The experimental data are well fit by a one-electron Nernst plot with a midpoint potential of -241 ± 20 mV *vs* NHE (pH 7.6). Further oxidation beyond -50 mV showed the formation of the characteristic "g = 2.02" signal of the oxidized $[Fe_3S_4]^+$ cluster.

VTMCD studies were carried out for a sample poised at -197 mV *vs* NHE in the presence of 55% (v/v) ethylene glycol to assess if one-electron oxidation occurs without loss of Zn^{2+}; see Figure 14. The resulting sample has temperature-dependent MCD bands throughout the UV/visible/near-IR region indicative of a paramagnetic Fe−S cluster. Moreover, while the pattern of negative and positive MCD bands shows some similarity to

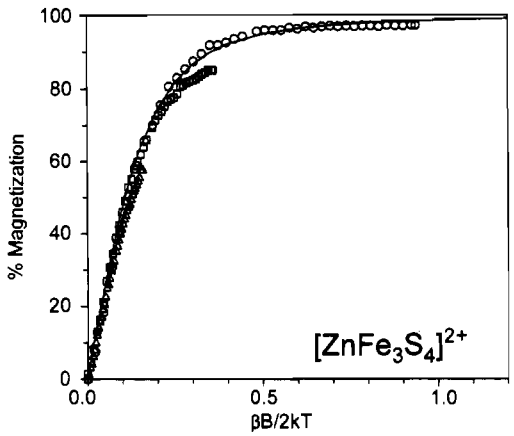

Figure 15. MCD magnetization plots for the $[ZnFe_3S_4]^{2+}$ cluster in thionin-oxidized *P. furiosus* Fd. The sample is as described in the caption of Figure 14. MCD magnetization was done at 770 nm. Temperatures: ○, 1.62 K; □, 4.22 K; △, 9.55 K. Magnetic fields were between 0 and 4.5 T. The solid line is for the theoretical magnetization data, constructed using eq 3 of ref 40, for an *xy*-polarized transition originating from an isolated doublet ground state with $g_{\parallel} = 8.00$ and $g_{\perp} = 0.00$.

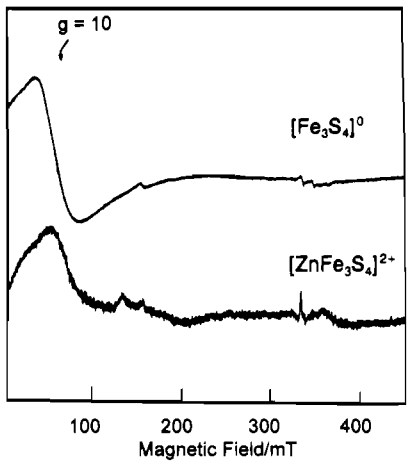

Figure 16. Comparison of the perpendicular mode X-band EPR spectra of the $[Fe_3S_4]^0$ and $[ZnFe_3S_4]^{2+}$ clusters in *P. furiosus* Fd. Spectra were recorded at 10 K; microwave power, 50 mW; microwave frequency, 9.43 GHz; modulation amplitude, 0.63 mT. The samples used are described in the captions of Figures 2 and 14, respectively.

that of the $S = 2$ $[Fe_3S_4]^0$ in *P. furiosus* Fd, it is quite different in terms of the wavelength of discrete transitions; *cf.* Figures 2 and 14. For example, the intense positive band centered around 708 nm, which is a characteristic feature of all $[Fe_3S_4]^0$ clusters, has shifted to 770 nm. Such perturbation of the electronic spectrum provides convincing evidence for one-electron oxidation of the Fe−S fragment to the $[Fe_3S_4]^0$ core oxidation state with retention of Zn^{2+}, i.e. the presence of a $[ZnFe_3S_4]^{2+}$ cluster. Low-temperature MCD spectra have been reported for the $[ZnFe_3S_4]^{2+}$ and $[CdFe_3S_4]^{2+}$ clusters in *D. africanus* FdIII.[10] The spectra are similar to those reported here except for smaller red shifts in the positive low-energy MCD band (712 nm for the $[Fe_3S_4]^0$ cluster in *D. africanus* FdIII compared to 727 and 732 nm for the $[ZnFe_3S_4]^{2+}$ and $[CdFe_3S_4]^{2+}$ clusters, respectively). These smaller shifts may be intrinsic to the clusters in this Fd or may be a consequence of mixtures of $[Fe_3S_4]^0$ and $[ZnFe_3S_4]^{2+}$ or $[CdFe_3S_4]^{2+}$ clusters coupled with the overlap of the underlying MCD spectrum of the inherent $S = {}^1/_2$ $[Fe_4S_4]^{1+}$ cluster that is present in *D. africanus* FdIII.

The effect of Zn^{2+} incorporation on the ground state properties of the $S = 2$ $[Fe_3S_4]^0$ cluster was investigated by MCD magnetization and EPR studies; see Figures 15 and 16, respectively. One-electron oxidation of the $[ZnFe_3S_4]^+$ cluster in *P. furiosus* Fd occurs with loss of the $[ZnFe_3S_4]^+$ resonance and the concomitant appearance of a broad low-field EPR signal centered around $g = 10$. The spectrum is similar to that observed for the $[Fe_3S_4]^0$ cluster in *P. furiosus*, and both are attributed to resonance within the lowest $M_s = \pm 2$ "doublet" of an $S = 2$ ground state with $D < 0$ since they increase in intensity with decreasing temperature down to 4.2 K. This is confirmed by MCD magnetization studies conducted at 770 nm for the $[ZnFe_3S_4]^{2+}$ cluster in *P. furiosus* Fd. The data are indistinguishable for the $[Fe_3S_4]^0$ and $[ZnFe_3S_4]^{2+}$ clusters, and in both cases, the lowest temperature data are well fit by theoretical data constructed for an *xy*-polarized transition from a doublet state with $g_{\parallel} = 8.0$ and $g_{\perp} = 0.0$. These are the effective *g*-values for an $M_s = \pm 2$ doublet of an axial $S = 2$ system. Hence the ground state properties of the $[Fe_3S_4]^0$ cluster are not significantly perturbed by the incorporation of Zn^{2+} and both exhibit $S = 2$ ground states with $D < 0$.

As was the case for the $[CoFe_3S_4]^{2+}$ cluster, ligand-binding experiments with the $[ZnFe_3S_4]^{2+}$ cluster were unsuccessful. One-electron oxidation of the cyanide- or thiolate-bound $[ZnFe_3S_4]^{2+}$ cluster and addition of a 10-fold excess of cyanide or 2-mercaptoethanol to the preformed $[ZnFe_3S_4]^{2+}$ cluster each resulted in samples containing a mixture of $S = 2$ $[Fe_3S_4]^0$ and $S = {}^1/_2$ $[Fe_3S_4]^+$ clusters as judged by parallel VTMCD and EPR studies. This is rationalized in terms of exogenous ligand binding at the Zn site followed by extraction as a result of the lower affinity of the $[Fe_3S_4]^0$ fragment for Zn^{2+} compared to the $[Fe_3S_4]^-$ fragment.[10]

Discussion

The combination of EPR, VTMCD, and absorption spectroscopies has been used in this work to establish the properties and ligand-binding capabilities of $[MnFe_3S_4]^+$, $[CoFe_3S_4]^{2+,+}$, and $[ZnFe_3S_4]^{2+,+}$ heterometallic cubane clusters assembled in *P. furiosus* Fd. The observed ground state properties of each of these clusters, both as prepared and after binding exogenous ligands, together with those of previously reported $[MFe_3S_4]^{2+,+}$ clusters (M = Fe, Ni, Tl) in *P. furiosus* Fd are summarized in Table 1. Overall, the results extend and reinforce the concept of cubane-type $[Fe_3S_4]^{+,0,-}$ clusters as redox-active, quasi-rigid cluster ligands for heterometal ions. In the $[Fe_3S_4]^+$ oxidation state, the electrophilic nature of the Fe(III) ions renders the three μ_2-S atoms insufficiently nucleophilic to bind hard divalent metal ions. However, $[Fe_3S_4]^{+,0}$ clusters are capable of binding soft monovalent metal ions such as Tl^+ and Cu^+.[17-19] In contrast, although it has yet to be observed in isolation, the $[Fe_3S_4]^-$ fragment readily binds to a variety of divalent and trivalent metal ions such as Zn^{2+},[9-11] Co^{2+},[12,13] Ni^{2+},[13-15] Cd^{2+},[10,13,16] and Ga^{3+}.[15] The present work adds Mn^{2+} to this list. In some cases, these clusters can be oxidized by one electron with retention of the heterometal ion or the $[MFe_3S_4]^{2+}$ cluster is formed directly on addition of divalent metal ion to the $[Fe_3S_4]^0$ cluster if the $[MFe_3S_4]^{2+,+}$ midpoint potential is lower than that of dithionite, e.g. $[ZnFe_3S_4]^{2+,+}$ and $[CdFe_3S_4]^{2+,+}$ clusters in *D. africanus* FdIII.[10] On the basis of kinetic evidence, Faridoon et al.[41] recently reported the formation of $[MFe_3S_4]^{2+}$ clusters (M = Mn, Co) in mitochondrial aconitase, but there is as yet no direct spectroscopic evidence for the formation or core oxidation state of these clusters. All of the available data indicate that affinity of the $[Fe_3S_4]^0$ fragment for divalent metal ions is greatly decreased compared to that of the $[Fe_3S_4]^-$ fragment.[10,17]

(41) Faridoon, K. Y.; Zhuang, H.-Y.; Sykes, A. G. *Inorg. Chem.* **1994**, *33*, 2209−2212.

Table 1. Summary of the Predicted and Observed Ground State Properties of $[MFe_3S_4]$ Clusters in *P. furiosus* Fd

cluster	metal ion		cluster fragment		ground state		ref
	M^{n+}	spin state[a]	oxidn state	spin state	predicted[b]	observed	
$[Fe_4S_4]^+$	Fe^{2+}	2	$[Fe_3S_4]^-$	$^5/_2$	$^1/_2$	$^1/_2$, $^3/_2$	20
$[Fe_4S_4]^+$–CN^-	Fe^{2+}	2	$[Fe_3S_4]^-$	$^5/_2$	$^1/_2$	$^1/_2$	25
$[Fe_4S_4]^{2+}$	Fe^{2+}	2	$[Fe_3S_4]^0$	2	0	0	20
$[ZnFe_3S_4]^+$	Zn^{2+}	0	$[Fe_3S_4]^-$	$^5/_2$	$^5/_2$	$^5/_2$	11, *c*
$[ZnFe_3S_4]^+$–CN^-	Zn^{2+}	0	$[Fe_3S_4]^-$	$^5/_2$	$^5/_2$	$^5/_2$	*c*
$[ZnFe_3S_4]^+$–RS^-	Zn^{2+}	0	$[Fe_3S_4]^-$	$^5/_2$	$^5/_2$	$^5/_2$	*c*
$[ZnFe_3S_4]^{2+}$	Zn^{2+}	0	$[Fe_3S_4]^0$	2	2	2	*c*
$[NiFe_3S_4]^+$	Ni^{2+}	1	$[Fe_3S_4]^-$	$^5/_2$	$^3/_2$	$^3/_2$	11, 14
$[NiFe_3S_4]^+$–CN^-	Ni^{2+}	1	$[Fe_3S_4]^-$	$^5/_2$	$^3/_2$	$^3/_2$	11, 14
$[CoFe_3S_4]^+$	Co^{2+}	$^3/_2$	$[Fe_3S_4]^-$	$^5/_2$	1	1	*c*
$[CoFe_3S_4]^+$–CN^-	Co^{2+}	$^3/_2$	$[Fe_3S_4]^-$	$^5/_2$	1	1	*c*
$[CoFe_3S_4]^{2+}$	Co^{2+}	$^3/_2$	$[Fe_3S_4]^0$	2	$^1/_2$	$^1/_2$	*c*
$[MnFe_3S_4]^-$	Mn^{2+}	$^5/_2$	$[Fe_3S_4]^-$	$^5/_2$	0	0	*c*
$[TlFe_3S_4]^+$	Tl^+	0	$[Fe_3S_4]^0$	2	2	2	18
$[TlFe_3S_4]^{2+}$	Tl^+	0	$[Fe_3S_4]^+$	$^1/_2$	$^1/_2$	$^1/_2$	18

[a] Assuming high spin. [b] Assuming antiferromagnetic coupling between high-spin metal ion, M^{n+}, and the cluster fragment. [c] This work.

Mössbauer and EPR studies of heterometallic clusters have been important for understanding the intracluster magnetic interactions of Fe–S centers. By the utilization of diamagnetic heterometal ions such as Zn^{2+}, Cd^{2+}, and Ga^{3+}, the $[Fe_3S_4]^-$ fragment has been shown to have an $S = ^5/_2$ ground state, which arises from antiparallel interaction between a valence-delocalized Fe^{2+}/Fe^{3+} pair ($S = ^9/_2$) and a valence-localized Fe^{2+} site ($S = 2$).[9-11,15,16] By analogy with the case of $[Fe_3S_4]^0$ clusters in bacterial Fds,[42] one-electron oxidation to yield a $[Fe_3S_4]^0$ cluster fragment is considered to occur at the localized valence site. The resultant $S = 2$ ground states of the $[CdFe_3S_4]^{2+}$ and $[ZnFe_3S_4]^{2+}$ clusters in *D. africanus* FdIII[10] and the $[ZnFe_3S_4]^{2+}$ cluster in *P. furiosus* Fd that have been identified by VTMCD studies are therefore presumed to arise from antiparallel interaction between the delocalized pair ($S = ^9/_2$) and the localized Fe^{3+} site ($S = ^5/_2$).

Prior to the present work, the ground state properties of heterometallic cubanes in Fds involving paramagnetic heteroatoms had only been established for $[CoFe_3S_4]^{2+}$ ($S = ^1/_2$) and $[NiFe_3S_4]^+$ ($S = ^3/_2$) centers. In both cases, the ground state spin can be rationalized on the basis of antiferromagnetic coupling between the high-spin metal ion and the appropriate cluster fragment,[8,32,43] i.e. Ni^{2+} ($S = 1$) coupled to $[Fe_3S_4]^-$ ($S = ^5/_2$) and Co^{2+} ($S = ^3/_2$) coupled to $[Fe_3S_4]^0$ ($S = 2$); see Table 1.[44] Of particular note is that the ground states of the two additional examples reported in this work are also predicted by this coupling scheme, i.e. Mn^{2+} ($S = ^5/_2$) coupled to $[Fe_3S_4]^-$ ($S = ^5/_2$) to yield a $[MnFe_3S_4]^+$ cluster with an $S = 0$ ground state and Co^{2+} ($S = ^3/_2$) coupled to $[Fe_3S_4]^-$ ($S = ^5/_2$) to yield a $[CoFe_3S_4]^+$ cluster with an $S = 1$ ground state; see Table 1. The latter is consistent with the preliminary Mössbauer data for the $[CoFe_3S_4]^{2+}$ cluster in *D. gigas* FdII which indicated a paramagnetic integer-spin ground state, $S \geq 1$.[12] The only ground state that is not correctly predicted by this simple scheme is the $S = ^3/_2$ form of the $[Fe_4S_4]^+$ cluster in *P. furiosus* Fd; see Table 1. However, recent ^1H NMR studies indicate a $S = ^1/_2$ ground state exclusively for this cluster in aqueous solution at room temperature, suggesting that the $S = ^3/_2$ ground state is a freezing artifact.[22] Moreover, the majority of biological $[Fe_4S_4]^+$ clusters exhibit $S = ^1/_2$ ground states exclusively, and the anomalous $S = ^3/_2$ form of the mixed-spin $[Fe_4S_4]^+$ cluster in *P. furiosus* Fd is quantitatively converted into an $S = ^1/_2$ form in frozen solutions on binding ligands such as cyanide and thiolates at the unique Fe site.[23,25,45]

Further evidence in support of this simple coupling scheme comes from the VTMCD spectra of each of the paramagnetic $[MFe_3S_4]$ clusters investigated thus far, i.e. $[Fe_4S_4]^+$ clusters[20,30,31,34] in a wide range of proteins; $[NiFe_3S_4]^+$,[45] $[CoFe_3S_4]^{2+,+}$ (this work), $[ZnFe_3S_4]^{2+,+}$ (this work), and $[TlFe_3S_4]^+$ [18] in *P. furiosus* Fd; and $[CuFe_3S_4]^+$,[19] $[ZnFe_3S_4]^{2+}$,[10] and $[CdFe_3S_4]^{2+}$ [10] in *D. africanus* FdIII. Each has an intense positive MCD band between 700 and 800 nm that does not correlate to a distinctive feature in the absorption spectrum. Recent studies from this laboratory indicate that this feature is the hallmark of a valence-delocalized $S = ^9/_2$ $[Fe_2S_2]^+$ unit and suggest assignment to an Fe^{2+}/Fe^{3+} intervalence band.[46] Such units are considered to be integral components of both the $[Fe_3S_4]^0$ and $[Fe_3S_4]^-$ fragments.

The ligand-binding properties of synthetic heterometallic and homometallic cubanes have been extensively investigated by Holm and co-workers.[8] In contrast, studies of exogenous ligand binding to similar clusters in biological environment have been confined to the $[Fe_4S_4]^{2+,+}$ clusters in aconitase,[3a,b] *P. furiosus* Fd,[23,25,45] and *D. africanus* FdIII[26] and to $[NiFe_3S_4]^+$clusters in *P. furiosus* Fd.[11,14,45] Throughout the present work, reversible changes in the EPR and VTMCD spectra of the $[MFe_3S_4]$ clusters in *P. furiosus* Fd (M = Zn, Co) induced by the addition of large excesses of cyanide or thiolate have been interpreted in terms of exogenous ligand binding at the unique metal site. An alternative explanation for the changes in spectroscopic properties is that large excesses of these exogenous ligands

(42) (a) Emptage, M. H.; Kent, T. A.; Huynh, B. H.; Rawlings, J.; Orme-Johnson, W. H.; Münck, E. *J. Biol. Chem.* **1980**, *255*, 1793–1796. (b) Huynh, B. H.; Moura, J. J. G.; Moura, I.; Kent, T. A.; LeGall, J.; Xavier, A. V.; Münck, E. *J. Biol. Chem.* **1980**, *255*, 3242–3244.

(43) Conover, R. C.; Finnegan, M. G.; Park, J.-B.; Adams, M. W. W.; Johnson, M. K. *J. Inorg. Biochem.* **1991**, *43*, 245.

(44) This simplified description of the intracluster magnetic interactions is used in Table 1. On the basis of the available Mössbauer data[32] and the VTMCD data presented in this work, which suggest the presence of an $S = ^9/_2$ delocalized Fe^{2+}/Fe^{3+} pair in each of paramagnetic heterometallic cubanes investigated (see text), a better description is likely to be that the ground state spin results from antiparallel coupling of a delocalized Fe^{2+}/Fe^{3+} pair ($S = ^9/_2$) with the parallel coupled heterodimer, i.e. M^{2+}(high spin) coupled to Fe^{3+}($S = ^5/_2$) for an $[MFe_3S_4]^{2+}$ cluster or Fe^{2+}($S = 2$) for an $[MFe_3S_4]^+$ cluster. The resultant ground state is the same, since the spin states of the $[Fe_3S_4]^0$ ($S = 2$) and $[Fe_3S_4]^-$ ($S = ^5/_2$) fragments, $S = 2$ and $^5/_2$, respectively, result from antiparallel coupling of a delocalized Fe^{2+}/Fe^{3+} pair ($S = ^9/_2$) with a localized-valence Fe^{3+} ($S = ^5/_2$) or Fe^{2+} ($S = 2$) site. In addition, it should be noted that Mössbauer studies of $[NiFe_3S_4]^+$ clusters, both synthetic and assembled in Fds,[11,32] indicate that the unique Fe site has an oxidation state between +3 and +2. This suggests partial delocalization with the Ni site which therefore must have an oxidation state between +2 and +1. The observed spin state ($S = ^3/_2$) can be reconciled with either of the two extremes, i.e. Ni^+ ($S = ^1/_2$) coupled to $[Fe_3S_4]^0$ ($S = 2$) or Ni^{2+} ($S = 1$) coupled to $[Fe_3S_4]^-$ ($S = ^5/_2$), and the reality probably lies somewhere between.

(45) Conover, R. C. Ph.D. Thesis, University of Georgia, Athens, GA, 1993.

(46) Crouse, B. R.; Meyer, J.; Johnson, M. K. *J. Am. Chem. Soc.*, in press.

Table 2. Comparison of the Reduction Potentials (mV *vs* NHE) for Synthetic and Biological Homometallic and Heterometallic $[MFe_3S_4]^{2+,+}$ Clusters

origin	$[Fe_3S_4]^{+,0}$	$[Fe_4S_4]^{2+,+}$	$[CdFe_3S_4]^{2+,+}$	$[ZnFe_3S_4]^{2+,+}$	$[CoFe_3S_4]^{2+,+}$	$[NiFe_3S_4]^{2+,+}$	$[MnFe_3S_4]^{2+,+}$	ref
P. furiosus Fd[a]	−160	−345	n.a.[b]	−241	−163	>−100	>−100	27, this work
D. gigas FdII[c]	−130	−420	−495	n.a.	−245	−360	n.a.	13
D. africanus FdIII[d]	−140	−400	−590	−480	n.a.	n.a.	n.a.	10
$[MFe_3S_4(Smes)_4]^{2-,3-}$[e]	n.a.	−1200	n.a.	n.a.	−1020	−900	n.a.	32

[a] Determined by dye-mediated EPR titrations at pH 8.0 ($[Fe_3S_4]^{+,0}$ and $[Fe_4S_4]^{2+,+}$) or pH 7.6 ($[MFe_3S_4]^{2+,+}$, M = Zn, Co, Ni, Mn). [b] Not available. [c] Determined by direct electrochemistry (square-wave voltammetry) at a glassy carbon electrode at pH 7.6. [d] Determined by cyclic voltammetry of a co-adsorbed film and in bulk solution at pH 7.0. [e] Determined by cyclic voltammetry in acetonitrile.

perturb the protein structure. However, two pieces of evidence provide compelling evidence in favor of the former explanation. First, precedent for this behavior comes from spectroscopic studies of the $[Fe_4S_4]^+$ cluster in *P. furiosus* Fd in the presence of excess cyanide. In this case, ^{13}C-ENDOR studies have provided definitive evidence that the changes in spectroscopic properties result from the binding of a single cyanide at the non-cysteinyl-coordinated Fe site. Second, the same excesses of cyanide or 2-mercaptoethanol as those used in this work were found to have absolutely no effect on the EPR and VTMCD spectra of the $[Fe_3S_4]^0$ and $[Fe_3S_4]^+$ clusters in *P. furiosus* Fd, both of which are devoid of the unique metal site.

The EPR and MCD results presented here are clearly consistent with reversible binding of exogenous ligands to the unique Zn subsite of the $[ZnFe_3S_4]^+$ cluster in *P. furiosus* Fd. The coordination of cyanide and 2-mercaptoethanol results in subtle but distinctive changes in the electronic and magnetic properties of the cluster while preserving the $S = {}^5/_2$ ground state. Of particular importance is that the thiolate-bound $[ZnFe_3S_4]^+$ cluster in *P. furiosus* Fd has electronic and magnetic properties similar to those of the $[ZnFe_3S_4]^+$ cluster in *D. gigas* FdII and *T. litoralis* Fd,[24] indicating cysteinyl sulfur coordination at the Zn site in these proteins. Thus far, exogenous ligand binding to homometallic and heterometallic cubane-type clusters in a biological environment has only been observed for clusters with non-cysteinyl coordination at a unique metal site. While further work is necessary, it is tempting to speculate that this is an obligate requirement for functionalization of this type of cluster in biology.

The cyanide-induced changes in the VTMCD spectrum of the $[CoFe_3S_4]^+$ cluster reported herein are fully reversible and comparable to those observed for the $[Fe_4S_4]^+$,[25] $[NiFe_3S_4]^+$,[45] and $[ZnFe_3S_4]^+$ (this work) clusters in *P. furiosus* Fd. In these cases, parallel EPR studies have confirmed that cyanide binding results in near-homogeneous species, since the cyanide-bound species each exhibit distinctive EPR state properties; see Figure 7 and refs 11, 14, and 25. Hence we conclude that the VTMCD data provide strong evidence for reversible cyanide binding to the $[CoFe_3S_4]^+$ cluster in *P. furiosus* Fd. Since analogous excesses of cyanide have no effect on the VTMCD properties of the $[Fe_3S_4]^0$ and $[Fe_3S_4]^+$ clusters in *P. furiosus* Fd,[24] this indicates that cyanide binding is localized at the Co site. Cyanide binding to the $[CoFe_3S_4]^+$ cluster occurs with retention of the $S = 1$ ground state and, therefore, does not induce a spin state change at the Co site. By analogy with the $[Fe_4S_4]^+$ cluster in *P. furiosus* Fd,[23] it seems likely that a single cyanide binds in place of a protein ligand to preserve approximately tetrahedral coordination at Co.

There are currently no examples of synthetic clusters containing $[CoFe_3S_4]^+$ cores. In contrast, there are one well-characterized biological example (in *D. gigas* FdII)[12] and two structurally characterized synthetic examples ($[CoFe_3S_4(R)_4]^{2-}$ where R = Smes[32] and Stib[33]) which contain $[CoFe_3S_4]^{2+}$ cores. However, the $[CoFe_3S_4]^{2+}$ cluster in *P. furiosus* Fd differs in one important respect, namely carboxylate rather than thiolate Co coordination. Hence differences in the EPR properties of the $[CoFe_3S_4]^{2+}$ clusters in *P. furiosus* Fd compared with those established for the synthetic clusters and in *D. gigas* FdII are likely to be indicative of differences in Co coordination. In accord with this hypothesis, the three clusters considered to have complete cysteinyl-*S* ligation have almost indistinguishable EPR signals, g = 1.98−1.99, 1.94, 1.82−1.81 with resolved hyperfine interaction only on the low-field component, 4.4 mT.[12,32,33] While the magnitude and anisotropy of the ^{59}Co hyperfine interaction (4.3 mT) for the $[CoFe_3S_4]^{2+}$ cluster in *P. furiosus* Fd are not significantly perturbed, the resonance is more axial with a substantially smaller g value anisotropy, g = 1.94, 1.87, 1.86. It was not possible to verify that these differences in the EPR spectra result exclusively from thiolate Co coordination, since attempts to add exogenous thiolate to the $[CoFe_3S_4]^{2+}$ cluster in *P. furiosus* Fd resulted in removal of the Co^{2+} and the concomitant formation of $[Fe_3S_4]^{+,0}$ clusters.

There are now sufficient examples of $[MFe_3S_4]^{2+,+}$ cubane clusters in synthetic and biological systems to permit comparison of the trends in reduction potentials as a function of the divalent metal ion, M. The data are summarized in Table 2. For the $[MFe_3S_4]^{2+,+}$ couples in *P. furiosus* Fd, the potentials increase in the order M = Fe < Zn < Co < Ni or Mn. Reversible one-electron oxidation was not possible for the $[MnFe_3S_4]^+$ clusters. However, redox titrations gave no evidence of oxidation at potentials up to −100 mV and progressive removal of the exogenous metal with formation of $[Fe_3S_4]^+$ clusters at higher potentials. Analogous behavior has been observed for the $[NiFe_3S_4]^+$ cluster in *P. furiosus* Fd.[45] Such behavior is to be expected for $[MFe_3S_4]^{2+,+}$ heterometallic clusters with potentials higher than that of the $[Fe_3S_4]^{+,0}$ couple (−160 mV in *P. furiosus* Fd) since the equilibrium

$$[MFe_3S_4]^{2+} \rightleftharpoons M^{2+} + [Fe_3S_4]^0$$

will be driven to the right by oxidation of the $[Fe_3S_4]^0$ cluster to the $[Fe_3S_4]^+$ form, which has very low affinity for divalent metal ions. While the potentials are much lower for the $[MFe_3S_4(Smes)_4]^{2-,3-}$ couples in acetonitrile, the order M = Fe < Co < Ni and the increase in potential for M = Co relative to M = Fe (180 mV) are the same as in *P. furiosus* Fd. However, this trend in potentials does not appear to be preserved in the other two Fds, for which redox data are available. The potentials increase in the orders M = Cd < Fe < Ni < Co in *D. gigas* FdII[13] and M = Cd < Zn < Fe in *D. africanus* FdIII.[10] These differences presumably relate to the cluster environment, and interpretation will certainly require additional data for a wider range of $[MFe_3S_4]^{2+,+}$ clusters in each Fd and high-resolution structural data for the *P. furiosus* Fd and *D. africanus* FdIII.

Acknowledgment. This work was supported by a grant from the National Institutes of Health (GM45597 to M.W.W.A. and M.K.J.). We thank Drs. Kristene Surerus and Eckard Münck for supplying the sample of *D. gigas* FdII containing a $[ZnFe_3S_4]^+$ cluster for VTMCD studies.

IC950610D